Aust. J. Phys., 1991, **44**, 545–63

Design of Support Pillar Arrays in Flat Evacuated Windows

R. E. Collins and A. C. Fischer-Cripps

School of Physics, University of Sydney,
Sydney, N.S.W. 2006, Australia.

Abstract

Flat evacuated glazing consists of two plane sheets of glass separated by a narrow evacuated space. These structures must incorporate an array of support pillars in order to maintain the separation of the glass plates under the influence of atmospheric pressure forces. A design procedure is outlined for determining the dimensions of this pillar array. Two important constraints in the design process are the mechanical tensile stress on the outside of the glass plates near the pillar, and the thermal conductance through the array of support pillars. A third constraint arises because of stress concentration near the pillars on the inside of the window. Evacuated windows having usefully low values of thermal conductance through the pillar array and tolerably small levels of exterior tensile stress can only be produced if large stresses exist on the inside of the structure in the region of the glass plates near the support pillars. The implications of these stresses are discussed. It is concluded that it is possible to design a pillar array for which the localised tensile stresses and overall thermal conductance have usefully small values.

1. Introduction

The requirement for transparent thermally insulating glazing is well recognised in low energy building design. Heat transport through windows constitutes a significant part of the thermal load for buildings and is particularly serious in severe climates. The traditional approach for the reduction of this heat flow is to use double, or multiple glazings. Heat flow through such glazings is determined by the thermal conductance of the internal gas space, and by radiation between the plates. The separation of the glass plates is limited by the requirement that significant convective heat transport through the internal gas space should not occur. Substantial performance improvements can be achieved in principle if the space between the two glass sheets is evacuated. There are substantial technological difficulties in achieving this.

The practical possibility of producing flat evacuated windows has recently been demonstrated (Robinson and Collins 1989; Collins and Robinson 1991). Such windows consist of two sheets of glass enclosing an evacuated space. It is necessary to produce a hermetic (leak-tight) seal around the periphery, to evacuate the structure to pressures below about 10^{-3} Torr ($\equiv 0 \cdot 133$ Pa), and to allow for the effects of the atmospheric pressure forces on the exterior of the glass sheets.

0004-9506/91/050545$05.00

In order to prevent a flat evacuated window from collapsing under atmospheric pressure forces, it is necessary to include within the structure an array of support pillars. Collins and Robinson demonstrated a design using fused glass support pillars which enables windows to be constructed which survive the stresses associated with atmospheric pressure forces. The pillars are made from solder glass—a low melting point lead borate glass that has a coefficient of expansion which quite closely matches that of the soda–lime glass sheets. The pillars are melted and fused to the surface of the glass sheets during the same process for making the hermetic edge seal.

The design of the pillar array is critical to the success of evacuated window technology. Such a design requires consideration of two competing constraints. First, the pillars cause regions of stress concentration within the window, which can result in fracture of the glass. Second, the pillars consititute thermal contacts between the two glass sheets increasing the heat transport through the window. This heat flow must be kept below specified levels. Collins and Robinson have proposed a thermal conductance value for the pillar array of $0 \cdot 3 \ \mathrm{W\,m^{-2}\,K^{-1}}$ for which windows of useful insulating properties can be built. In combination with internal low emittance coating, a window containing such an array would have insulating properties at least twice as good as the best available double glazing.

Collins and Robinson developed a design approach for evacuated windows based on a trade-off between the maximum tensile stress on the inside of the glass adjacent to the pillars, and the maximum tolerable heat transport through the pillar array. This previous analysis draws heavily on earlier work by Benson *et al.* (1990). This approach defines the range of values of pillar separation and pillar radius for which these two constraints are satisfied. In order to minimise stresses elsewhere in the window, specifically on the outside of the glass sheets above the pillars, individual pillars in the window should be spaced as close together as possible. This design process therefore leads to a specification of one pillar separation and a corresponding pillar size.

The present paper further develops the design procedure for pillar arrays in evacuated windows. The current analysis uses as its primary design constraint the tensile stresses which exist in the glass plates on the outside near the pillars. Recent experimental work in our laboratory has demonstrated that such stresses dominate the failure mechanisms in the structures. The reason for this is that the exterior surfaces of the window are not protected. The glass can therefore be damaged by handling, causing the formation of surface flaws which result in concentration of the tensile stress. In addition, water vapour exists in significant quantities on the outside of the window and this results in the reduction of the surface energy of the glass and increases the probability of a fracture developing from the surface flaws. The approach outlined in this paper indicates that there is substantially more flexibility in the design of a pillar array than was suggested by Collins and Robinson.

2. Design Criteria

The three principal factors to be considered in the design for a pillar array in an evacuated window are: the thermal conductance of the pillar array; the mechanical tensile stresses within the interior of the window near the pillars;

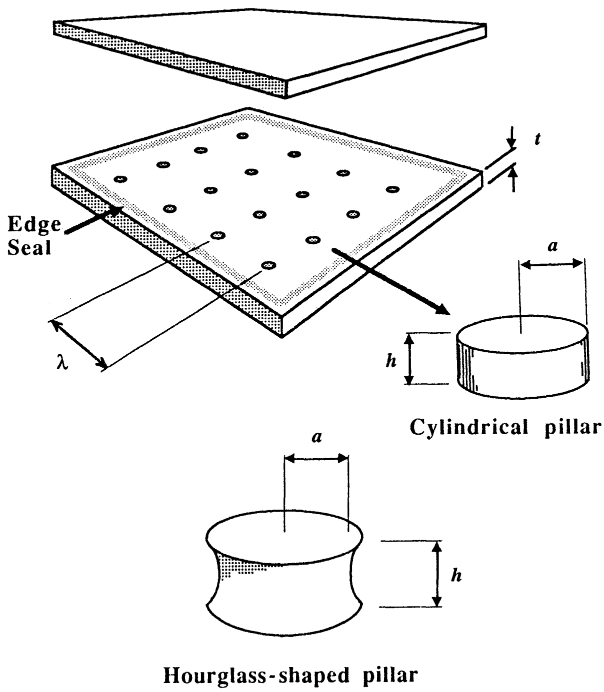

Fig. 1. Diagram of the pillar array in an evacuated window. Enlarged views are shown of a cylindrical pillar, and of an hourglass-shaped pillar which is formed from solder glass in practical evacuated windows.

and the mechanical tensile stresses on the exterior surfaces of the window near the pillars. We consider a window design consisting of two plane sheets of glass of thickness t separated by a periodic array of pillars on a square grid of separation λ (Fig. 1). Other array geometries (for example hexagonal) are possible, but this does not affect the general principles developed here. The pillars are initially assumed to be cylindrical with radius a and height h. However, in practical realisations of this window design, the pillars have an hourglass shape of the form shown in Fig. 1 due to the wetting of the glass plates by the solder glass during the high temperature fusion process. It turns out that, for pillars of this shape the mechanical stresses in, and near the pillars, are substantially less than for cylindrical pillars, as discussed below.

(a) Thermal Conductance of the Pillars

In a previous paper (Collins *et al.* 1991) an analysis was presented of the thermal conductance of pillars of cylindrical geometry. Briefly it was shown that, for very short pillars ($h \ll a$), the thermal conductance of an individual pillar between two essentially infinite glass plates is $2\kappa a$, where κ is the thermal conductivity of the glass (Holm 1979). The heat transport is determined by the 'spreading resistance' from the small diameter pillar into the bulk of the glass. Fig. 2a shows the isotherms within a window which clearly illustrate this effect. These data were obtained using a finite element calculation.

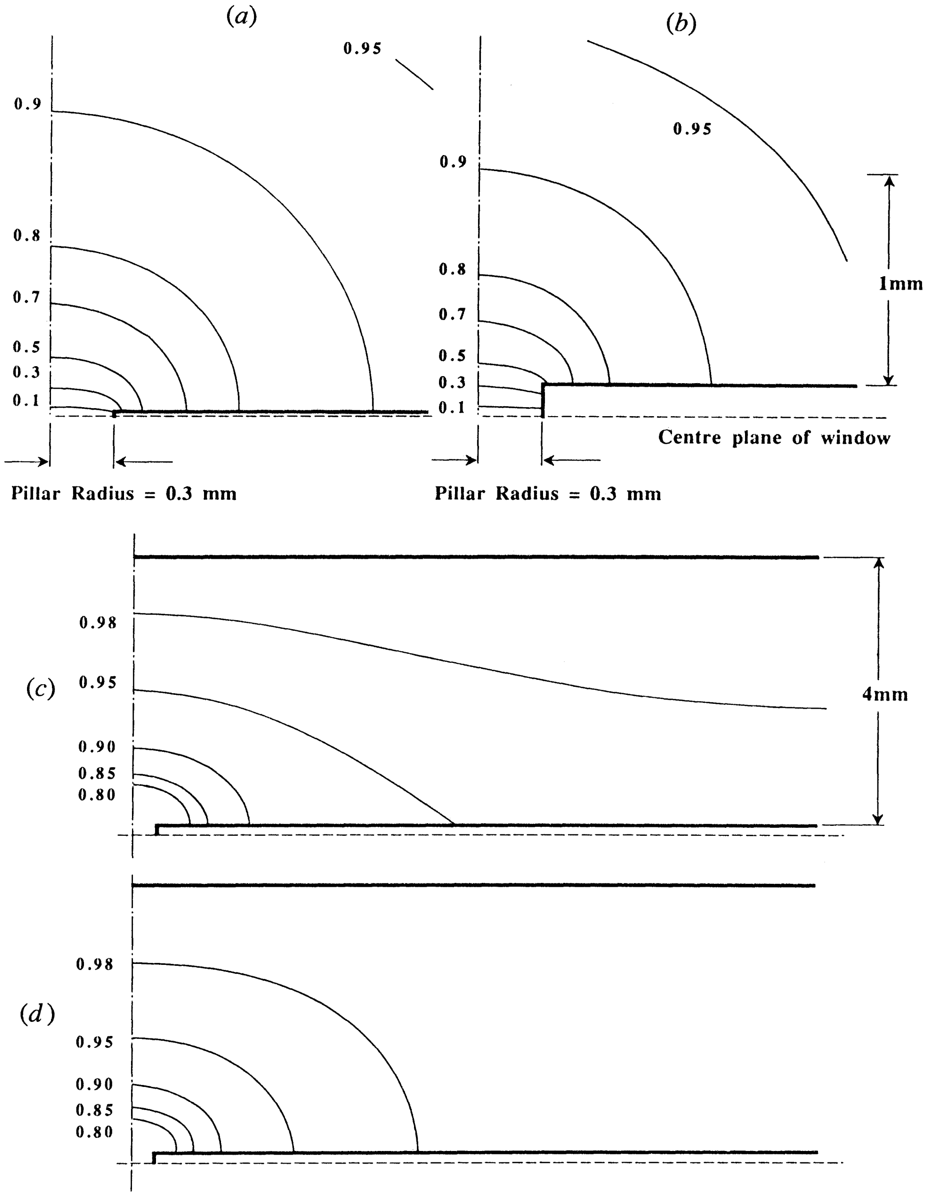

Fig. 2. Isotherms within an evacuated window in the region near a single cylindrical support pillar. Shown are data for (*a*) a very short pillar and (*b*) a pillar with height equal to its radius. The temperature difference from the outside surface to the mid-plane of the window is normalised to unity. The glass sheets are 4 mm thick. The isotherms are calculated using the thermal conductivity appropriate for soda–lime glass ($0 \cdot 78\ \mathrm{W\,m^{-1}\,K^{-1}}$). The emittance of the interior surface is taken to be $0 \cdot 1$. Thermal conductance of gas in the internal space is assumed to be negligible. Note the increased resistance for the case of a pillar with nonzero height. Parts (*c*) and (*d*) show some of the isotherms for windows with pillar height equal to the radius in which the emittance of the inner surface is $0 \cdot 84$ and $0 \cdot 10$ respectively. Despite the qualitative difference of the large-value isotherms, the thermal conductance of the pillar is essentially identical in each case.

For pillars of increasing height, the thermal conductance decreases due to the finite resistance of the pillar material itself. Fig. 2*b* shows the isotherms for a cylindrical pillar with height equal to the radius. Collins *et al.* (1991) presented data for thermal conductance of a pillar showing the effect of height over a restricted range. We have performed a finite element analysis of the heat flow through such pillars over an extended range of heights. The results are shown in Fig. 3, for pillars of different fixed height $h = 0$, $0{\cdot}05$, $0{\cdot}1$ and $0{\cdot}3$ mm, and glass sheets 4 mm thick.

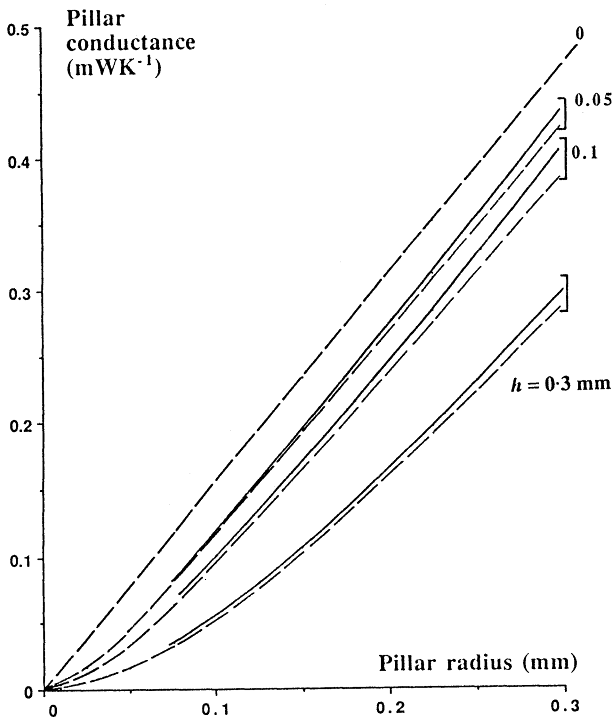

Fig. 3. Thermal conductance of individual cylindrical pillars separating two sheets of 4 mm thick soda–lime glass as determined by finite element modelling. Results are shown (full curves) for pillars of different fixed heights. The thermal conductivity of the pillar material is assumed to be the same as that of the bulk glass ($0{\cdot}78\ \mathrm{W\,m^{-1}K^{-1}}$). The dashed curves show the result obtained for series addition of the spreading resistance and the pillar resistance, assuming plane parallel heat flow in the pillar (see equation 1). Note the effect of a finite plate thickness at large radii in the finite element results, resulting in the curves departing from the classical analytical solution which assumes semi-infinite plate thickness.

As would be expected, the thermal impedance of an individual pillar of finite height is not too different from that which would be calculated from the simple addition of the spreading resistance in the glass plates and the resistance of the pillar itself, assuming plane parallel heat flow. In this approximation, we can write:

$$C_{\mathrm{pillar}} \approx 2\kappa a/(1 + 2h/\pi a). \qquad (1)$$

For comparison with the finite element result, this simple empirical relation is also shown in Fig. 3 by the dashed curves.

In the practical windows of interest, the pillar height can be controlled independently of radius. We can write the height in terms of the radius:

$$h = \xi a \,. \tag{2}$$

Equation (1) can then be rewritten as

$$C_{\text{pillar}} \approx 2\kappa a/(1 + 2\xi/\pi) \,. \tag{3}$$

In the samples constructed to date, the pillar height is approximately equal to the pillar radius ($\xi = 1$). We therefore use this geometry in our design process described below. We emphasise, however, that any desired aspect ratio may be selected and more complex pillar shapes can also be considered simply by determining the thermal conductance of the appropriate geometry.

(b) Internal Mechanical Stresses

The small total contact area of the pillars relative to the overall window size results in substantial concentration of stresses in the vicinity of the pillars. The internal stresses in the glass, immediately adjacent to the pillars, have been extensively studied in the context of Hertzian fracture experiments. In a classic work, Hertz (1881) calculated the stress distribution in glass sheets close to the area of contact of a spherical indenter. This geometry now forms the basis of a standard test procedure for determining surface energy of brittle materials, as it results in a well-controlled conical stress fracture near the indenter. The stress fields beneath such an indenter are complex (Lawn and Wilshaw 1975*a*, 1975*b*). Broadly speaking, however, the three principal stresses are compressive immediately beneath the indenter. Just outside the indenter, the surface of the indented material contains a radial tensile stress and a compressive hoop stress. It is the radial tensile stress which is responsible for the formation of the conical fracture. In addition, the third principal stress is compressive and orthogonal to the other two stresses. This stress is directed normally to the surface at the exterior surface, with a value of zero at the surface, and develops into a set of conical surfaces sweeping away from the indenter at an angle of approximately 68° to the normal. Fully developed fractures closely follow the geometry of this third principal stress.

The conditions under which a spherical indenter results in fracture in the indented material have been very extensively examined. It is now generally agreed (Frank and Lawn 1967; Langitan and Lawn 1969; Mouginot and Maugis 1985) that the fracture, when it occurs, initiates from a surface flaw in the brittle indented material close the region of maximum radial tensile stress on the surface, just outside the contact area. Two distinct modes of fracture exist. For surface flaws above a certain size, a very small ring crack first forms in the indented material, just outside the contact area of the indenter. This can occur at quite small applied forces. The location of the ring crack is determined by the size of the flaws, being closer to the indenter for smaller flaws (Mouginot and Maugis 1985). This crack is usually extremely difficult to see and is generally only observable using etching techniques. The ring crack is stable and remains quite small as the load on the indenter increases. Above a certain load, however, and depending on its radius, the ring crack grows unstably into a cone crack at a well-defined angle (approximately 68° to the normal) and to a well-defined depth. Because the magnitude of the stress fields falls off very rapidly with distance from the indenter, this cone crack is stable and does not result in catastrophic failure of the solid as a whole.

If there is no pre-existing flaw above a critical size in the vicinity of the indenter, the ring crack may not form until a very large force is applied. In this case its formation may occur simultaneously with that of the cone crack and the cone crack will then grow immediately to a well-defined size, determined by the force at the instant of fracture. The size of the cone crack is also affected by the surface energy of the glass. Indeed, the classical model for crack propagation in brittle materials developed by Griffith (1920) is based on the relative energies involved in the elastic deformation of the material, and the formation of additional surface area as the crack extends. The growth under constant load of conical Hertzian crack, subsequent to its initial formation, is therefore dependent on whether the surface energy remains constant. It is well known, however, that the presence of corrosive environments can lower the surface energy leading to further crack growth. The most important practical contaminant in this context is water vapour, which can result in a halving of surface energy. The affinity of water molecules for a very clean, freshly fractured glass surface is very large. Colloquially, we can say that the water molecules migrate to the tip of the crack and wedge the glass surfaces apart.

The stress corrosion effect has been extensively studied and is often the mechanism responsible for spontaneous fracture of glass in the field. In the context of the conical Hertzian fracture, the presence of water vapour results in the growth of the crack over a period of time. It is important to note, however, that with the geometry discussed here, crack growth eventually stops, because of the spatial distribution of the stress fields in the vicinity of the indenter.

An early development from Hertzian fracture experiments on glass was the observation that the force on the spherical indenter necessary to form a cone crack is proportional to the radius of the indenter over a wide range of conditions. This observation, made by Auerbach (1891), is one of the classical relationships in the study of the fracture of brittle materials. Auerbach's law was initially observed for spherical indenters. However, if the relationship is re-written in terms of the radius of the contact circle, it is found, within experimental error, that the same fracture criterion also applies for flat ended cylindrical indenters (Mouginot and Maugis 1985).

A considerable amount of work has been done aimed at explaining Auerbach's law. In one approach, it is assumed that the brittle material fails at a predetermined tensile stress. The magnitude of this stress at any point close to the indenter is determined by the macroscopic stress field, concentrated by pre-existing flaws in this region. However, in order to explain Auerbach's law in this way it is necessary to assume a quite specific statistical distribution of flaw sizes on the surface of the brittle material. The generality of Auerbach's law makes this explanation seem quite improbable.

An alternative fracture mechanics approach, pioneered by Frank and Lawn (1967) and further developed by Mouginot and Maugis (1985), explains Auerbach's law in terms of regions of stability and instability in the growth of the crack. This explanation was convincingly demonstrated to be correct by Langitan and Lawn (1969) in a series of classic experiments, in which a high density of surface flaws was introduced into the region which was subsequently stressed. They found that Auerbach's law held, independent of the size of the flaws, and explained these results in terms of the formation of the seminal ring crack; the existence of flaws results in the formation of the ring crack at quite low loads. The subsequent propagation of this ring crack into a cone crack is then independent of the pre-existing flaws and is determined only by the stability of the crack growth in the stress field. In the subsequent analysis we use the results of Langitan and Lawn and the explanations of Frank and Lawn (1967) and Mouginot and Maugis (1985) to develop design criteria relating to the formation of conical cracks in evacuated windows.

(c) External Mechanical Stresses

In addition to the high levels of radial tensile stress on the inside of an evacuated window near the pillars, the region close to the pillars on the outside of the glass sheets also experiences tensile stress. Calculations have shown (Timoshenko and Woinowsky-Krieger 1959) that this exterior tensile stress is much smaller than the interior stresses, typically by an order of magnitude or more. However, abrasion of the exterior surface of a window can result in the introduction of flaws which, when large enough, may develop into a fracture.

Further, it is well known that the presence of water vapour significantly reduces the fracture toughness of glass by lowering its surface energy and reacting chemically with the highly stressed bonds at the tip of a crack or flaw. A scratch which is below the critical flaw size for unstable fracture may extend slowly over a period of days or even years, finally reaching the critical size. Since the exterior of the evacuated window is not protected from water vapour, dust and abrasion, then an appopriate design constraint must include an allowance for sub-critical crack growth with reference to an acceptable expected lifetime.

In conventional glass installations, the maximum level of macroscopic tensile stress in glass, for which a negligible probability of fracture exists in service, is 8 MPa (H. W. McKenzie, personal communication, 1990). Here, as a conservative estimate, we take half this figure as a basis for a design constraint by examining the sub-critical crack growth behaviour of flaws for glass immersed in water. Such an analysis, following a procedure outlined by Davidge (1979), shows that for a constant applied stress of 4 MPa, and for a lifetime of 100 years, flaws less than 0·35 mm deep would be required.

Clearly this is an extremely conservative approach since it must be recognised that the high level of tensile stress only occurs in a very small area directly above each pillar, and it is unlikely that a window will be continually wet for this period. The conservative nature of this estimate is further reinforced when it is realised that the analysis is based on the existence of a very sharp flaw, and that the occurrence of suitably sharp flaws in the region of stress can only be described in probabilistic terms. Finally, sharp flaws 0·35 mm deep are exceedingly severe and unlikely to occur in normal service.

In the analysis presented below, we take 4 MPa as a conservative upper limit to the exterior tensile stress. This leaves some room for other induced stresses which are likely to occur in service, such as wind loads and thermal expansion.

There is a further region of tensile stress within the window which exists because of the bending of the glass plates between the pillars due to atmospheric pressure forces. This region is on the interior surfaces of the plates, in-between the pillars. However, it turns out (Timoshenko and Woinowsky-Krieger 1959) that the levels of stress in this region are about an order of magnitude less than those on the outside of the glass near the pillars. In any case, this interior surface is protected from damage and is in a water-free vacuum environment. These interior tensile stresses therefore do not constitute a significant constraint on the design of a pillar array and are not considered further here. Similarly, it is readily shown that bending deflections of the glass plates between the pillars are very small for the pillar separations discussed here, and do not impose a significant constraint on the design of evacuated windows.

3. Design Approach for a Pillar Array

The preceding discussion leads to a design procedure for determining the dimensions of a pillar array. Firstly, the separation of the pillars λ is determined so as to keep the external tensile stresses in the glass plates near the pillars below some predetermined design value. For small pillars, this stress is virtually independent of the pillar radius a, but such a dependence could be easily accommodated by iteration if necessary. Secondly, this value of λ, when combined with the design constraint of a maximum thermal conductance for the pillar array, defines the dimensions of individual pillars. There is some flexibility in the choice of a if pillars of significant height can be used. As noted, in our analysis we choose the pillar height h to be equal to a. Thirdly, the values of λ and a are used to determine whether a conical stress fracture is likely to occur through application of Auerbach's law. As will be shown, the likelihood of the occurrence of conical stress fracture is greatly reduced for the hourglass-shaped pillars used in our windows, compared with the case of cylindrical pillars. The fracture criterion based on Auerbach's law therefore significantly overestimates the possibility of such a fracture. Finally, the implications of a conical fracture are assessed in terms of visual impact, or catastrophic failure of the window. These steps are now discussed in detail.

(a) Maximum Tensile Stress above the Pillars

Timoshenko and Woinowsky-Krieger (1959) discussed the problem of a thin flat plate of thickness t under uniform load, supported by a square array of circular pillars of radius a and separation λ. From this analysis, we can derive a result for the maximum tensile stress in the plates on the loaded side:

$$B_{\max} = \frac{3q\lambda^2(1+\mu)}{2\pi t^2}\,[\ln(\lambda/a) - 0\cdot811]\,, \qquad (4)$$

where q is the loading pressure on the plate and μ is Poisson's ratio. The maximum deflection of the plates between the pillars is given by

$$\Delta y_{\max} = 0 \cdot 0697\, q\lambda^2(1-\mu^2)/Et^3\,, \tag{5}$$

where E is Young's modulus for the material.

Unfortunately, the thin plate result (4) does not give a particularly accurate estimate of maximum tensile stress in the glass plates because, in an evacuated window, the thickness of the plate is in general much greater than the pillar diameter. A comprehensive review of the literature has failed to find any calculation for the stresses in a periodically supported thick plate. However, a very good estimate of such stresses can be obtained by considering the cylindrically symmetric problem of a uniformly loaded thick disc with an opposing, localised force acting at the centre. Such a case differs from a unit cell of the periodically supported plate only at points far from the centre; it should therefore quite accurately reproduce the stresses near the pillars at the centre of our windows.

We first quote a relevant result from Timoshenko and Woinowsky-Krieger (1959), who gave an analytic solution for the central tensile stresses in a thick,

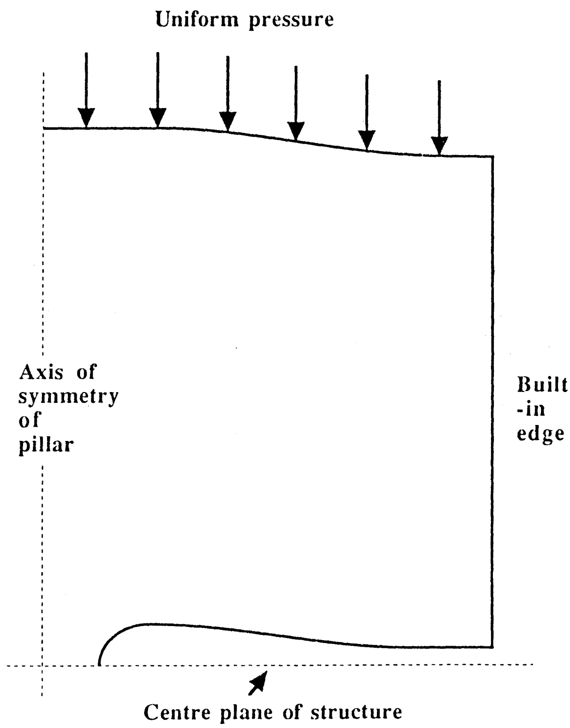

Fig. 4. Geometry of a circular section from an evacuated window structure used for finite element modelling of the stresses in the glass plates. The drawing is not to scale. The axial dimensions are greatly expanded, and the radius and height of the pillar are much larger than in a practical device, in order to illustrate the deflections and boundary conditions.

simply supported disc of thickness t and diameter λ, with a localised force $\pi q\lambda^2/4$ at the centre:

$$B_{\max} = \pi q\lambda^2[(1+\mu)\{0\cdot 485\ln(\lambda/2t) + 0\cdot 52\} + 0\cdot 48]/4t^2. \quad (6)$$

They also showed how to convert this case to a disc with built-in edges:

$$B_{\max} = \pi q\lambda^2(1+\mu)\{0\cdot 485\ln(\lambda/2t) + 0\cdot 52\}/4t^2. \quad (7)$$

This latter situation more accurately reproduces the edge boundary conditions of a unit cell of the periodically supported plate, but does not include the uniform loading inherent in the window structure.

We have utilised a finite element approach to model the stresses in the plate for each of these cases and obtained results for the stresses and deflection which are in good agreement with the analytic treatments. We can therefore, with confidence, apply the finite element approach to a situation which quite closely approximates a unit cell of the periodically supported plate. The system is shown in Fig. 4. Two circular discs, each with built-in edges, are separated by a single axial pillar, and compressed by a uniform external pressure acting over the surface of each disc. Fig. 5 shows values, calculated from this model, of the maximum tensile stress on the outside pressurised surfaces of the discs, as a function of the thickness of the disc, for various values of pillar

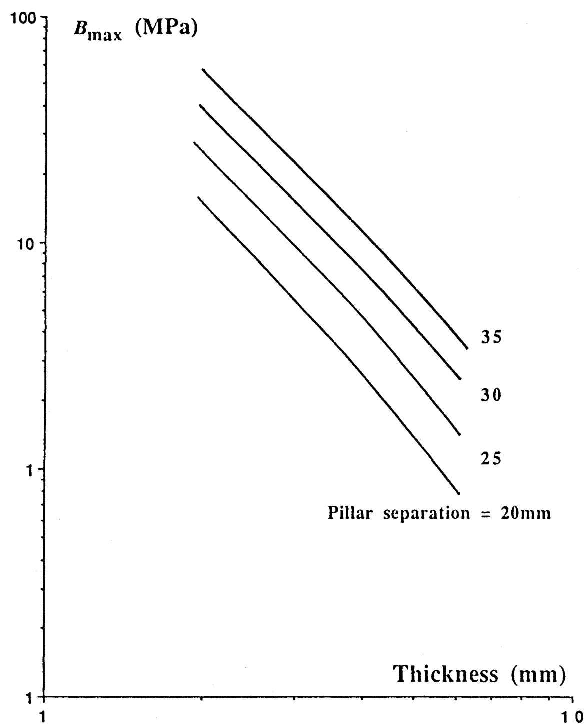

Fig. 5. Values of maximum external tensile stress close to the support pillar obtained by finite element analysis of the structure in Fig. 4. The localised force is taken to be that which acts on each unit cell of the evacuated window.

separation, chosen to be equal to the disc diameter. The external uniform pressure used in these calculations is scaled up from the atmospheric pressure value by a factor $4/\pi$, so that the force on the axial pillar is equal to that which would act on a pillar in the square array of separation λ. The calculated values of maximum tensile stress are found to be not too strongly dependent on the diameter of the disc, for constant central force. For example, for a 25 mm diameter, 4 mm thick disc, changing the diameter of the disc by 10% gives a variation of maximum tensile stress of about 6%, for constant axial force. This confirms our expectation that the stress obtained for the cylindrically symmetric case modelled here should be a good approximation to that in the periodically supported plate. As a point of interest, the values of stress calculated from the finite element approach are approximately one half those obtained from the thin plate formula (4).

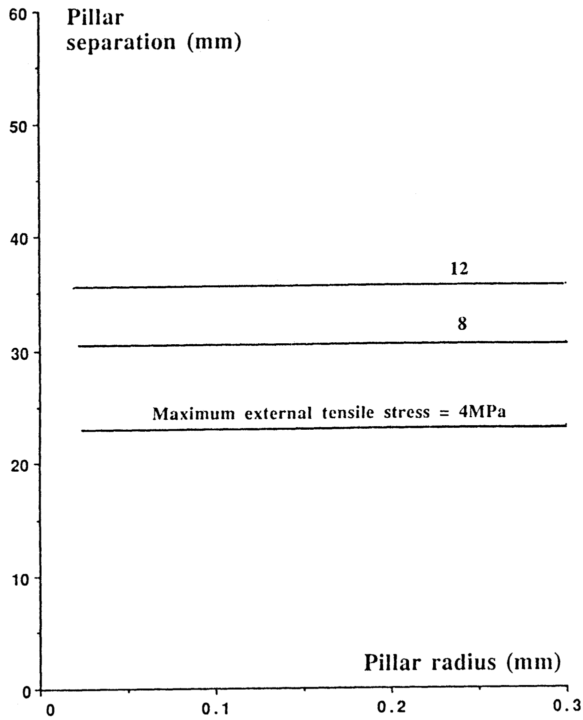

Fig. 6. Data for maximum external tensile stress close to a support pillar plotted on a graph of pillar separation λ versus pillar radius a. This graph serves to define regions of the (λ, a) plane for which the external tensile stress is below any specified value.

The results of Fig. 5 can be re-plotted on a graph of λ versus a, as shown in Fig. 6, with the maximum external stress as the variable. (In this graph a has practically no effect on the levels of stress in the plate on the opposite face.) In order to maintain the external tensile stress below some specified value, it is necessary to choose values for λ and a which lie below the line corresponding to this value of stress. This is the first design constraint for the dimensions of the pillar array.

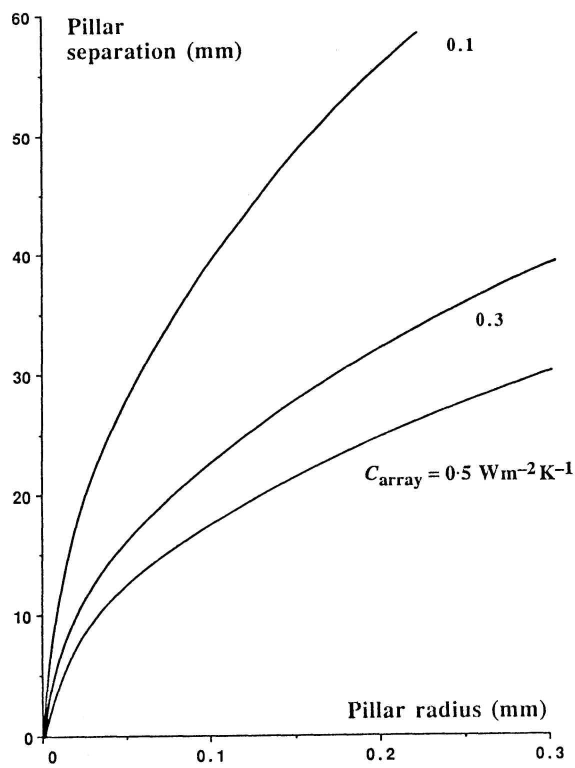

Fig. 7. Thermal conductance of a pillar array plotted on a graph of pillar separation λ versus pillar radius a. The data are obtained by a series addition of spreading resistance and pillar resistance of the heat flow through individual cylindrical pillars. Results are presented for pillars of zero height ($\xi = 0$). In order to satisfy the specification for thermal conductance of the pillar array, the (λ, a) point must lie above the relevant curve.

(b) Thermal Conductance of the Pillar Array

The thermal conductance of an individual pillar, C_{pillar}, may be used to calculate the thermal conductance of the entire array of pillars, C_{array}. For a square array of pillars of separation λ, there are $1/\lambda^2$ pillars per unit area, so we can write

$$C_{\text{array}} = C_{\text{pillar}}/\lambda^2 \,. \tag{8}$$

Writing the conductance of an individual pillar in the approximate analytic form (3), we can derive

$$\lambda^2 = 2\kappa a/(1 + 2\xi/\pi)C_{\text{array}} \,. \tag{9}$$

A similar non-analytic relationship can be calculated if we use the more accurate finite element result for the pillar conductance. In addition, other array geometries (e.g. hexagonal) result in minor modifications. The important conclusion to be drawn, however, is that a second relationship exists between

λ and a. This relationship is shown in Fig. 7 for cylindrical pillars of zero height ($\xi = 0$), and in Fig. 8 for cylindrical pillars with height equal to the radius ($\xi = 1$). In order to satisfy the specification for thermal conductance, the (λ, a) design point must lie above the relevant curve. The thermal conductance specification therefore defines a second region of the (λ, a) plane in which values of these two quantities may be chosen.

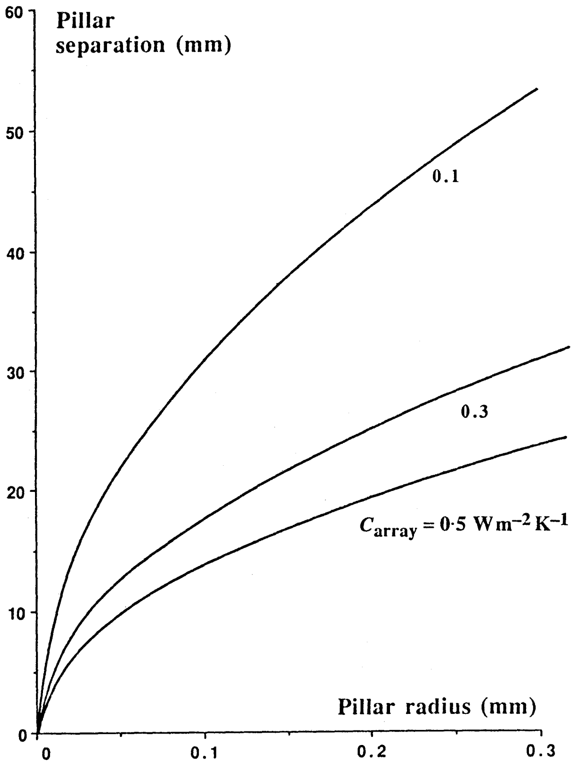

Fig. 8. As for Fig. 7, but for cylindrical pillars with height equal to radius ($\xi = 1$).

(c) Occurrence of Cone Fracture

Auerbach's law is an empirical relationship which describes the observed proportionality between the applied force P_c necessary to produce a conical fracture and the radius R of a spherical indenter:

$$P_c = AR. \tag{10}$$

The constant A is experimentally determined. Hertz (1881) calculated the radius a of the contact area of a spherical indenter on a surface:

$$a^3 = 4kPR/3E, \tag{11}$$

where P is the applied force, while k is a dimensionless constant involving Young's modulus E and Poisson's ratio μ:

$$k = 9/16[(1 - \mu_2^2) + (1 - \mu_1^2)E_2/E_1]. \tag{12}$$

The subscripts 1 and 2 represent the indenter and the indented material respectively. For similar materials with $\mu \approx 0 \cdot 33$, we get a value $k \approx 1$.

Combining (10) and (11), we can derive

$$P_c = (3AE/4k)^{1/2} a^{3/2}, \tag{13}$$

which is an alternative statement of Auerbach's law. It is now known that the linear dependence in this law on the radius of a spherical indenter is of no fundamental significance in itself. Equation (13) contains the essential functional dependences which can be related to the stress fields within the material. Moreover, the 3/2 power dependence of the fracture force on contact radius expressed in (13) is experimentally observed for both spherical and flat indenters over a wide range (the 'Auerbach range').

In this discussion we utilise previously measured values of the fracture force to predict the likelihood of formation of a conical stress fracture beneath a support pillar in an evacuated window. These data are for both spherical indenters (Langitan and Lawn 1969) and flat indenters (Mouginot and Maugis 1985). Langitan and Lawn performed measurements on abraded soda–lime glass, and Mouginot and Maugis used abraded borosilicate glass. Both investigations involved static loading, and Langitan and Lawn also studied fractures formed

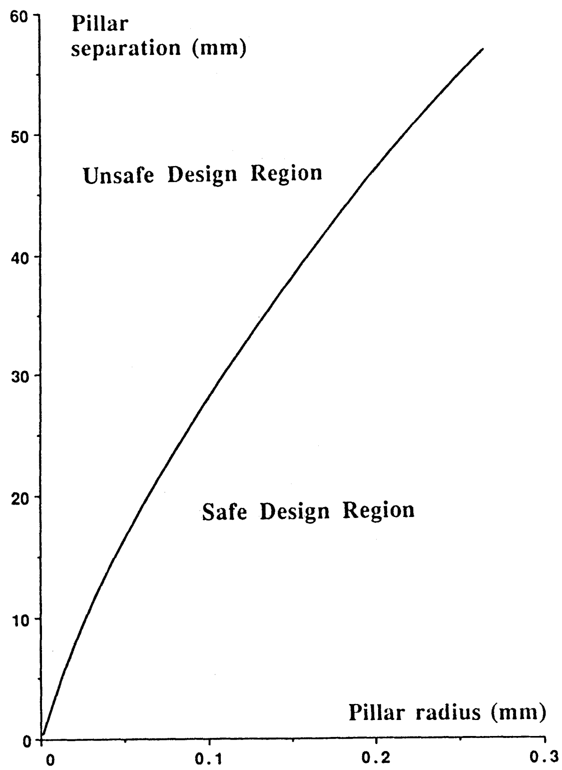

Fig. 9. Auerbach's law plotted on a graph of pillar separation λ versus pillar radius a. The curve is derived from data on spherical and flat indenters. If the (λ, a) point is chosen to lie below the curve, it is unlikely that a conical stress fracture will occur.

under impact loading. To the accuracy of the data (±10%), both static tests yield the result

$$P_c = 2400a^{3/2}, \tag{14}$$

where P_c is in Newtons and a in millimetres. For impact loading, the force necessary to initiate cone fracture was found to be nearly twice as large, reflecting the larger surface energy for crack formation in the absence of water vapour.

We can write the force on each pillar P_c in terms of the atmospheric pressure q and the pillar separation λ. For a square array we have

$$P_c = q\lambda^2. \tag{15}$$

Combining (14) and (15) gives

$$\lambda = 155a^{3/4}, \tag{16}$$

where λ and a are in mm. This third relationship between λ and a is shown in Fig. 9. For the stress levels in the vicinity of the pillar to be less than those leading to fracture according to Auerbach's law, the (λ, a) design point must lie below the curve.

As noted, the data used to derive (16) are for fractures on abraded glass. In such a case, it is virtually certain that the seminal ring crack exists at quite low applied forces and the fracture force values are those required to overcome the instability criterion in order that the cone fracture may develop. These values for force, therefore, represent a lower limit for the formation of the cone fracture. For surfaces which have a very low density of flaws, it is quite possible to achieve much higher values of force before the conical fracture occurs, because the ring crack may not be initiated. This is the situation which is expected to exist within evacuated window structures produced according to the methods described by Collins and Robinson (1991). In these structures, the pillars are made from solder glass which is melted and solidified during the process for formation of the edge seal. The surface of such freshly solidified glass is expected to be flaw-free. Moreover, because of the wetting of the glass plates by the solder glass during the high temperature process, the surface of the glass plates surrounding the pillar is also expected to be flaw-free. Finally, these surfaces are completely inaccessible, being on the interior, evacuated part of the window and are therefore not subject to mechanical damage. It is quite possible, therefore, that ring and cone fractures may never occur in the glass under the support pillars in windows made using these methods, even at force levels substantially greater than those given by Auerbach's law (16). The situation is not unlike that now routinely achieved in the manufacture of optical fibres; the pristine surface of the glass fibre is protected from damage immediately after its formation, preventing the occurrence of surface flaws, and thus resulting in a negligible probability of fracture over the entire service life, even to stresses well above values normally regarded as intolerable in glass structures. Finally, we have used the (conservative) result from static tests in which water vapour is known to encourage the formation of cracks.

The interior of evacuated windows should be essentially free of water vapour and it is probable that higher forces than those inferred from the static tests would be tolerable in this environment. We conclude, therefore, that the Auerbach criterion is a quite conservative predictor of the possibility of cone crack formation in evacuated windows.

Finite element calculations of the stress distributions in the vicinity of the hourglass-shaped pillars (Fig. 1) used in our windows show that the surface levels of radial tensile stress are very significantly reduced compared with the cases of spherical or flat indenters. It seems that the skirts of the shaped pillar act to reinforce the structure, spreading localised intense stress fields close to the circumference of the pillar, perhaps even 'steering' the axial compressive stress in the pillar into a radially outward direction in the glass plates. In addition, the mechanical bonding of the glass pillar to the glass plates appears to change qualitatively the shape of the stress fields in this region and also to reduce the levels of stress. These considerations further emphasise the conservative nature of the Auerbach criterion for formation of conical stress fracture.

Finally, Langitan and Lawn (1969) and Mouginot and Maugis (1985) provided data on the size of the conical stress cracks for the size range of indenters of interest here. It was found that such cracks are very small, perhaps twice the diameter of the pillar indenter, and they only propagate to a depth of about one third the radius of the pillar. In our own experimental work, we have never seen conical cracks beneath pillars unless local forces are applied which are many times the value normally experienced in practical windows. When such crack have been induced, they do not result in loss of the vacuum in the window. We therefore conclude that conical fractures due to concentrated stress fields in the glass adjacent to support pillars are unlikely to be of concern in the design of evacuated windows.

(d) Combination of Design Constraints

The previous analysis serves to define constraints, due to three effects (external tensile stress above the pillar, thermal conductance of the pillar array, and internal crack formation adjacent to the pillar), on the choice of values of λ and a in an evacuated window. These constraints are reproduced separately in Figs 10*a*, 10*b* and 10*c* showing the range of (λ, a) for which each is satisfied. The graphs are combined in Fig. 10*d* to show the range of (λ, a) which satisfy all these design constraints. We note that the allowed values of λ and a depend on the actual design specifications. For example, Fig. 10 has been drawn for $C = 0\cdot3\ \mathrm{W\,m^{-2}\,K^{-1}}$, for a rectangular array of cylindrical pillars with height equal to radius, and for an external tensile stress of 4 MPa. The procedures described here permit any other design specifications to be used. The important conclusion to be drawn is that there is a range of (λ, a) which satisfy all these design criteria.

The choice of specific (λ, a) values within the allowable range is very much determined by technological considerations, which will not be discussed in detail here. However, we note that factors which may influence the chosen design values include: the method of production of the pillars; the number of pillars that can be made economically; the minimum desirable gap in the windows; the visibility of the pillars; and the minimum pillar size that can be conveniently produced. For example, if it is desired to minimise the number of pillars, because they are deposited individually, then an appropriate choice to satisfy the above design constraints would be $\lambda = 23$ mm, $a = 0 \cdot 17$ mm. If, however, pillars are deposited collectively, by screen printing for example, other factors may lead to a choice of different values within the allowable range.

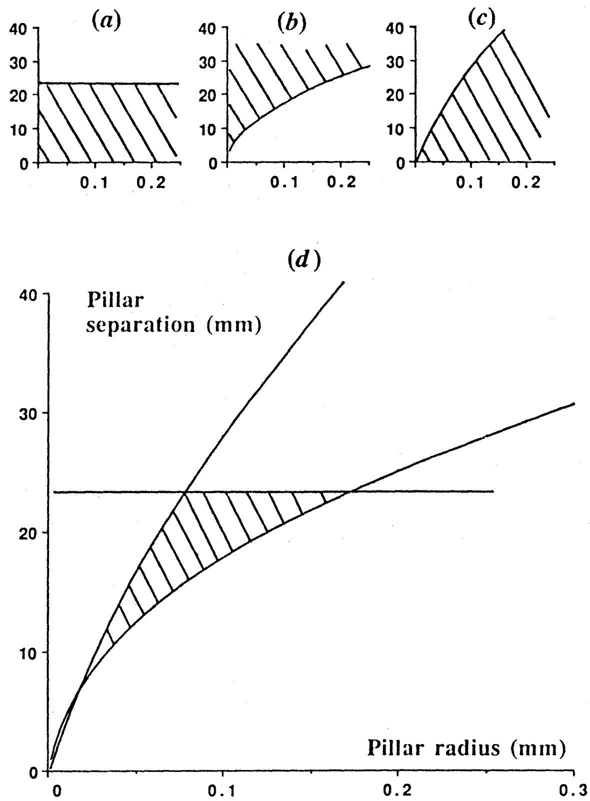

Fig. 10. Combination of the design constraints for a pillar array. Figs 10*a*, 10*b* and 10*c* are reproductions of Figs 6, 8 and 9 and show respectively (λ, a) and values which satisfy the following design constraints: external tensile stress is less than 4 MPa; thermal conductance of the pillar array is below $0 \cdot 3$ W m^{-2} K^{-1}; and conical stress fracture is unlikely to occur. Fig. 10*d* combines these three relationships to show (λ, a) values for which all three design constraints are satisfied. These results are for a square array of cylindrical pillars with height equal to radius.

4. Conclusions

The analysis presented here has considered several factors which restrict the dimensions of an array of support pillars in all-glass evacuated windows. It has been shown that a pillar array can be designed having very small conductive heat flow through the pillars ($<0 \cdot 3$ W m^{-2} K^{-1}), and for which fracture due to mechanical stresses caused by atmospheric pressure is extremely unlikely. The analysis has been deliberately conservative; in several of the arguments presented a 'worst case' scenario has been used. There is substantial scope for refinement of the design process, particularly by developing a more complete analysis of the probability of fracture due to external stresses, and of the nature of stresses in the immediate vicinity of the shaped pillars. Both refinements are expected to increase the range of permissible design values for the pillar array.

It is important to extend the analysis to include the influence of shear stresses and barrel distortion in the support pillars. Shear stresses will arise from non-uniform wind loading, and the existence of such stresses could be an important limitation on pillar dimensions. Preliminary modelling work has indicated that the magnitude of barrel stresses is quite dependent on the shape of the pillars, with quite low stresses existing in the hourglass-shaped pillars in our windows. The assessment of the importance of these two effects will also require a detailed study of the mechanical properties of the solder glass, about which very little appears to have been reported.

Acknowledgments

Helpful discussions are acknowledged with H. W. McKenzie of Pilkington, United Kingdom. This work was supported in part by His Royal Highness Prince Nawaf bin Abdul Aziz of the Kingdom of Saudi Arabia through the Science Foundation for Physics within the University of Sydney and by the Energy Research and Development Corporation.

References

Auerbach, F. (1891). *Ann. Phys. Chem.* **43**, 61.

Benson, D. K., Smith, L. K., Tracy, C. E., Potter, T., Christensen, C., and Soule, D. E. (1990). Vacuum window glazings for energy efficient buildings: Summary Report. Internal Report Number SERI/TP-212-3684. Solar Energy Research Institute, Golden, Colorado, USA.

Collins, R. E., Poladian, L., Pailthorpe, B. A., and McPhedran, R. C. (1991). *Aust. J. Phys.* **44**, 73.

Collins, R. E., and Robinson, S. J. (1991). Evacuated glazing. *Solar Energy* **47**, 27.

Davidge, R. W. (1979). 'Mechanical Behaviour of Ceramics' (Cambridge Univ. Press).

Frank, F. C., and Lawn, B. R. (1967). *Proc. R. Soc. Lond.* A **299**, 291.

Griffith, A. A. (1920). *Phil. Trans. R. Soc. Lond.* A **221**, 163.

Hertz, H. (1881). *J. Reine Angew. Math.* **92**, 156. [Reprinted in English in Hertz Miscellaneous Papers, Ch. 5 (Macmillan, 1896).]

Holm, R. (1979). 'Electric Contacts—Theory and Application', 4th edn (Springer: Berlin).

Langitan, F. B., and Lawn, B. R. (1969). *J. Appl. Phys.* **40**, 4009.

Lawn, B. R., and Wilshaw, T. R. (1975*a*). 'Fracture of Brittle Solids' (Cambridge Univ. Press).

Lawn, B. R., and Wilshaw, R. (1975*b*). *J. Mat. Sci.* **10**, 1049.

Mouginot, R., and Maugis, D. (1985). *J. Mat. Sci.* **20**, 4354.

Robinson, S. J., and Collins, R. E. (1989). Evacuated windows—Theory and practice. Proc. ISES Solar World Congress, Kobe, Japan (Pergamon: Oxford).

Timoshenko, S., and Woinowsky-Krieger, S. (1959). 'Theory of Plates and Shells', 2nd edn (McGraw–Hill: New York).

Manuscript received 6 March, accepted 7 June 1991